Journal of Mechanical Research and Application (JMRA), Vol. 11 No.3, 1400(2021),76-99

3D CFD investigation on thermal performance of a U-tube borehole heat exchanger

Ali Abjadi[*1] ,Mohammadreza Asadbeigi[2], Shayan Farjyar[3] Farzad Ghafoorian[4],

[1] Department of Mechanical Engineering, South Tehran Branch, Islamic Azad University, Tehran, Iran.
[2] School of Mechanical Engineering, Iran University of Science and Technology, Tehran, Iran.
[3] Department of Civil Engineering, Architecture and Art, Islamic Azad University, Science and Research branch,Tehran,Iran
[4] Turbomachinery Research Laboratory, Department of Energy Conversion, School of Mechanical Engineering, Iran University of Science and Technology, Tehran, Iran.

Received: 2022-08-22 **Accepted**: 2022-011-12

Abstract

In the current numerical simulation study, a special configuration of geothermal heat exchangers called U-tube borehole heat exchangers was analyzed by using computational fluid dynamics (CFD) method. This system is made of a U-shaped pipe, where the water flow enters from one side and exits from the other side after exchanging thermal energy. These heat exchangers are used for heating and cooling applications. The studied system is for cooling the working fluid. The U-shaped pipe inside the borehole, which has a depth equal to the height of the pipe, is embedded in dense materials such as cement. The type of materials used as backfill for heat exchange is very important because their physical and thermal properties are effective in the process of heat transfer between the soil and the working fluid inside the heat exchanger. Based on the CFD results, it was determined that grout improves heat transfer and system efficiency due to its thermal conductivity. Also, the inlet mass flow rate, which is effective on the working fluid velocity, Reynolds number and pressure drop, was evaluated and it was found that with the increase of the inlet mass flow rate, the performance of the system improves, meaning that a mass flow rate of 0.5 (kg/s) caused a further increase in the borehole wall temperature, which indicates more reduction in working fluid temperature over the time.

Keywords: *U-tube borehole heat exchanger; computational fluid dynamics; backfill thermal conductivity; pressure drop; Reynolds number*

Nomenclature			
Symbols		**Subscript**	
C_p	Specific heat capacity (J/kg.K)	m	Porous medium
P	Pressure (Pa)	s	Solid pipe wall
T	Water outlet temperature (K)	w	Water
R	Thermal resistance (m.K/W)	g	Groundwater
h	convective heat transfer coefficient of the circulating fluid (W/m^2K)	i	Inner pipe
k	Hydraulic conductivity (lit/s)	o	Outer pipe
V_f	Darcy velocity (m/d)	f	Fluid
H	Hydraulic head (m)	p	Particle of nanofluid
ṁ	Mass flow rate (kg/s)	nf	Nanofluid
U	Effective velocity (m/s)	bf	Base fluid
Re	Reynolds number of the circulating fluid	**Abbreviations**	
Pr	Prandtl number	TRT	Thermal response test
t	Time (hour)	BHE	Borehole heat exchanger
Greek		GSHP	Ground source heat pump
θ	Porosity	RANS	Reynolds averaged Naiver Stokes
α	Thermal diffusivity (m^2/s)	HDPE	High-density polyethylene
λ	Thermal conductivity (W/m.K)	PVC	Polyvinyl chloride PVC
ρ	Density (Kg/m^3)	CFD	Computational fluid dynamics
φ	Volume fraction(%)		
μ	Dynamic viscosity(Kg/m.s)		

1. Introduction

Increasing concerns about global warming and environmental pollution, as well as deficiency and limitation in fossil energy, increased interest in renewable energy. Clean fuel resources such as

wind, solar, hydroelectric power, geothermal and biomass are reliable alternatives to fossil fuels [1]. Geothermal energy can be one of the appropriate alternative options. This energy is essentially free from NOx and SO2 release and other destructive environmental enclosures. Geothermal energy is economical in areas with suitable geographical features and over 50,000 GWh of electricity is generated by this method[2]. In recent years, one of the ways to use geothermal energy is a ground source heat pump (GSHP), which has been considered by many researchers[3]. Borehole heat exchangers (BHE) are one of the most important components of geothermal heat pumps, which are now widely used to protect energy in the heating and cooling of buildings[4]. Geothermal power plants and heat pumps can work in combination with solar power plants to generate adequate electricity power[5]. Recently, this technology and energy source has been used in hydrogen production cycles and the results showed that it was economically viable[6]. Also, heat pumps have been widely used for the ventilation of classrooms and buildings due to their good efficiency in heat recovery cycles[7]. Different geometries are used for the borehole heat exchanger. One or two U-tubes may be placed in a vertical borehole. This type of heat exchanger has been widely used due to its ease of installation as well as low maintenance costs[8]. Other different designs that have coaxial pipe geometries or geometries involving several pipes around an internal pipe have been designed and operated industrially[9]. Also, helical geometries have been of special interest due to their lower drilling depth and consequently lower cost [10]. In Iran, the study of geothermal heat exchangers has recently become popular. Old abandoned oil and gas wells can be used as geothermal sources to extract energy. In recent years, a simulation of a coaxial geothermal heat exchanger has been performed on two abandoned oil wells with specific temperatures in Ahvaz[11]. The most important advantage of U-tube-shaped heat exchangers over coaxial and helical types is their higher heat exchange surface[12]. In general, the space between

the soil and the system pipes is often filled with grout. One of the effective ways to improve the performance of these energy storage systems has been to change the type of grout around the pipes to play the role of thermal insulation in a more effective way[13]. To achieve this goal, the thermal and physical properties of the grout, such as thermal conductivity, specific heat capacity and porosity, are changed[14]. There are different approaches to study thermal behaviour inside and around U-tube borehole heat exchangers, including experiments, numerical simulations, and analytical models. In the field of experimental studies, the thermal response test (TRT) method for estimating soil thermal performance and investigating soil thermal parameters in the design of borehole heat exchangers has been considered[15]. In addition to research applications, this test is also considered to determine the appropriate location for the installation of heat exchangers[16]. This method determines the heat transfer properties of borehole heat exchangers according to the difference between inlet and outlet temperatures. This experiment has been performed by many researchers to investigate the temperature distribution along the pipe[17]. Since the initial cost of experimental studies with borehole heat exchangers has been very high, many researchers have turned to software analysis and computational fluid dynamics (CFD) analysis for heat transfer analysis[18]. Various methods have been proposed to improve performance and increase the temperature during geothermal heat exchangers. To achieve this goal, it is possible to make changes in the geometry of the pipes, change the type and speed of the working fluid and use the appropriate material to insulate around the heat exchanger pipes[19]. One of the common changes in the geometry of the pipes is the addition of fins to increase the contact surface and thus increase the heat transfer level and ultimately improve the efficiency of the system[20]. Also, the thermal efficiency of the system was evaluated by applying changes to the diameter and thickness of the inlet pipe[21]. Also, the distance between the inlet and outlet sections of the U-tube BHE was

changed and by performing a TRT test on it, the appropriate distance between the inlet and outlet sections was obtained[22]. Since the material of pipes and their thermal properties have a significant role in thermal efficiency, the effect of different materials on thermal efficiency was investigated and the results showed that High-density polyethylene (HDPE) and Polyvinyl chloride (PVC) can be a suitable choice for design BHEs[23]. In some cases, to increase the efficiency, two or more U-tube pipes are buried together in the soil. In this case, the distance between the pipes has been very important[24]. As mentioned, working fluid plays a very important role in the thermal performance of BHEs. Therefore, to investigate this issue, the inlet fluid was sent into the inlet pipe with different velocities or mass flow rates[25]. Similarly, the duration of fluid presence in BHE was changed. This numerical simulation was performed by Transient method [26]. The results showed that with increasing velocity, the working fluid is exposed to geothermal energy for a shorter time, thus it leads to a drop in the rate of increase of working fluid temperature along the pipe[27]. On the other hand, the type of working fluid and its physical and thermal properties have a significant effect on thermal efficiency, so to increase the efficiency of the system, nanofluids are used instead of pure water[28]. In addition to geometric parameters and selection of optimal operating conditions for the appropriate working fluid, soil conditions around the system also play a vital role in system efficiency[29]. Studies have shown that the presence of groundwater, which is a natural and unavoidable phenomenon, and its seepage into the soil of the area and the contact of BHE pipes with groundwater flow significantly reduces the efficiency[30].

In this study, a sample of U-shaped BHEs was evaluated by CFD. The operation of this heat exchanger is based on heat transfer between a liquid working fluid such as water with a higher temperature than the surrounding soil. Hot water enters from one side of the U-tube and with the

passage of time, it is placed near the soil with a lower temperature, and finally, by losing its thermal energy, it leaves with a lower temperature. Effective parameters such as the effect of the inlet mass flow rate on the process of heat transfer and pressure drop inside the pipe and the effect of the backfill material on improving the heat transfer are investigated by observing the increase in the borehole wall temperature.

2. Physical model and geometry

In the present study, a U-tube BHE is considered as the prototype. The working method of this geothermal heat exchanger is that the operating fluid with a certain temperature and mass flow rate enters from the inlet section of the U-tube pipe and after passing the path of the U-shaped pipe, it leaves the outlet edge. Obviously, during the fluid flow inside the heat exchanger, heat transfer takes place between the working fluid and the surrounding soil. In the hot seasons when the surrounding soil temperature is higher than the working fluid, the system is used for water heating. In cold seasons, this operation is reversed and this system is used for water cooling. BHE system consists of a big cylindrical model as the surrounding soil, a smaller cylinder as the borehole drilled in the soil which is often filled with cement, and a U-shaped pipe in which the working fluid flows. The dimensions of the soil layers in a front view are shown in Figure 1 and the dimensions of other components of the BHE system are also given in Table 1. These dimensions have been used before by Kim et al[31].

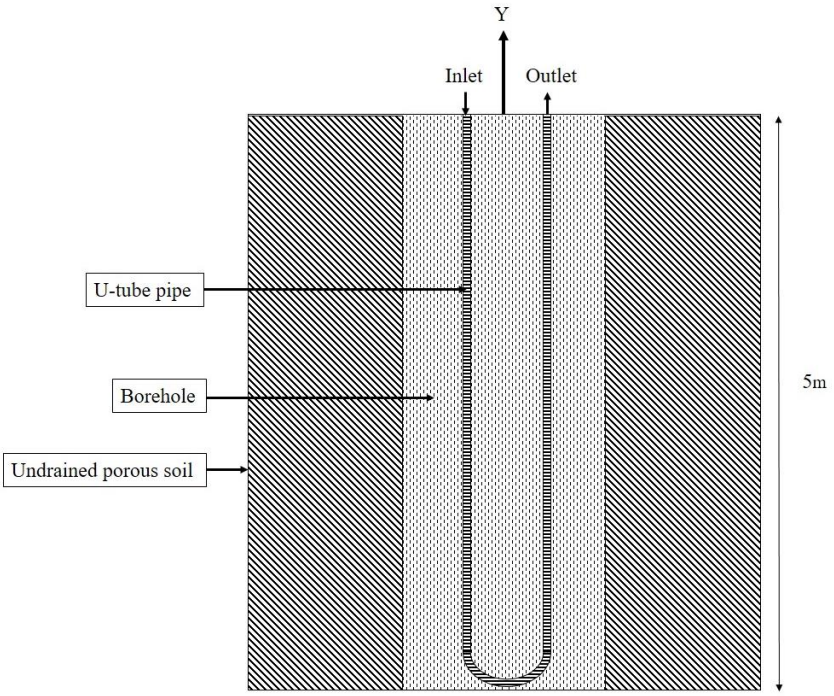

Figure 1 BHE front view

Table 1 Geometrical parameters

	Quantity	Value
1	Borehole diameter	0.110(m)
2	Soil diameter	6.000(m)
3	External U-tube diameter	0.032(m)
4	U-tube distance (center to center)	0.060(m)
5	Borehole length	5.000(m)
6	U-tube length	5.000(m)
7	Soil domain length	5.000(m)

In the studied BHE system, HDPE is considered a U-tube pipe material. Also, the inside of the borehole space is filled with grout. These properties have been selected according to the study of Kim et al[31]. The physical and thermal properties of the BHE system components are given in Table 2.

Table 2 Thermal and physical properties of materials

	Quantity	Value
1	Water density	998.2(kg/m3)
2	Water specific heat	4182(J/kg.K)
3	Water thermal conductivity	0.6(W/m.K)
4	Pipe density	940(kg/m^3)
5	Pipe specific heat	2000(J/kg.K)
6	Pipe thermal conductivity	0.48(W/m.K)
7	Soil density	2650(kg/m^3)
8	Soil specific heat	815(J/kg.K)
9	Soil thermal conductivity	3.5(W/m.K)
10	Backfill density	2400 (kg/m3)
11	Backfill specific heat	1627 (J/kg.K)
12	Backfill thermal conductivity	1.3 (W/m.K)

3. Mathematical model

3.1. Fluid mechanic and turbulent flow equations

For numerical simulation, Ansys Fluent analytical software is used, which drives Reynolds averaged Naiver Stokes (RANs) equations to analyze fluid flow. The general form of these equations is as follows:

$$\frac{\partial \overline{u_i}}{\partial x_i} = 0 \text{ [32]} \tag{1}$$

$$\rho\left[\overline{u_j}\frac{\partial \overline{u_i}}{\partial x_j}\right] = -\frac{\partial \overline{P}}{\partial x_i}\left[\mu\left(\frac{\partial \overline{u_i}}{\partial \overline{x_j}}\right) - \rho\overline{u_i'}\overline{u_j'}\right] \text{[32]} \tag{2}$$

$$\rho c_p \overline{u}_j \frac{\partial \overline{T}}{\partial x_j} = \frac{\partial}{\partial x_j}\left[\lambda\left(\frac{\partial \overline{T}}{\partial \overline{x}_j}\right) - \rho \overline{u'_j T'}\right] \text{ [32]} \quad (3)$$

Also, the basic general equation of transport, which describes the principle of mass, momentum, and energy conservation, is written as follows:

$$\frac{\partial}{\partial t}(\rho\phi) + \frac{\partial}{\partial x_j}(\rho U \phi) = \frac{\partial}{\partial x_j}\left(\Gamma_\phi \frac{\partial \phi}{\partial x_j}\right) + S_\phi \text{ [33]} \quad (4)$$

$$\frac{\partial}{\partial t}(\rho U) + \mathrm{div}(\rho . \mathrm{U} . \mathrm{U}) = \mathrm{div}(\mu_{eff} . \mathrm{gradU}) - \frac{\partial p}{\partial x} + \frac{\partial}{\partial x}\left(\mu_{eff} . \frac{\partial U}{\partial x}\right) + \frac{\partial}{\partial y}\left(\mu_{eff} . \frac{\partial V}{\partial x}\right) + \frac{\partial}{\partial z}\left(\mu_{eff} . \frac{\partial W}{\partial x}\right) \quad [33] \quad (5)$$

$$\frac{\partial}{\partial t}(\rho V) + \mathrm{div}(\rho . \mathrm{V} . \mathrm{V}) = \mathrm{div}(\mu_{eff} . \mathrm{gradV}) - \frac{\partial p}{\partial y} + \frac{\partial}{\partial x}\left(\mu_{eff} . \frac{\partial U}{\partial y}\right) + \frac{\partial}{\partial y}\left(\mu_{eff} . \frac{\partial V}{\partial y}\right) + \frac{\partial}{\partial z}\left(\mu_{eff} . \frac{\partial W}{\partial y}\right) \quad [33] \quad (6)$$

$$\frac{\partial}{\partial t}(\rho W) + \mathrm{div}(\rho . \mathrm{W} . \mathrm{W}) = \mathrm{div}(\mu_{eff} . \mathrm{gradW}) - \frac{\partial p}{\partial z} + \frac{\partial}{\partial x}\left(\mu_{eff} . \frac{\partial U}{\partial z}\right) + \frac{\partial}{\partial y}\left(\mu_{eff} . \frac{\partial V}{\partial z}\right) + \frac{\partial}{\partial z}\left(\mu_{eff} . \frac{\partial W}{\partial z}\right) \quad [33] \quad (7)$$

In the above equations, $\partial/\partial t\,(\rho\phi)$ is the foreign exchange rate, $\partial/\partial x_j\,(\rho U \phi)$ is flow of convection, $\partial/\partial x_j\,(\Gamma_\phi(\partial\phi/\partial x_j))$ is flow of diffusion and S_ϕ is the source term.

Due to the geometry of the pipe and the velocity of the inlet fluid, the Reynolds number has been greater than 2000; therefore, turbulent flow in the U-shaped pipe is considered. The RNG k-ε turbulence model is used to simulate the turbulent flow because this model has acceptable accuracy and also it can increase numerical solution speed. Also in order to model turbulent flow at low

velocities and Reynolds numbers, model RNG k-ε offers a differential equation based on an analytical solution for effective viscosity, thus mentioned model is shown more accuracy than k-ε standard and k-ω turbulence models [34]. The equations of turbulent kinetic energy transport (k) and the rate of dissipation (ε) are as follows:

$$\frac{\partial}{\partial t}(\rho k)+\frac{\partial}{\partial x_i}(\rho . k U_i)=\left(\left(\frac{\partial}{\partial x_j}\mu+\frac{\mu_t}{\sigma_k}\right)\frac{\partial k}{\partial x_j}\right) \quad [35] \quad (8)$$
$$+G_k+G_b-\rho\varepsilon+S_k$$

$$\frac{\partial}{\partial t}(\rho\varepsilon)+\frac{\partial}{\partial x_i}(\rho . \varepsilon U_i)=\frac{\partial}{\partial x_j}\left(\left(\mu+\frac{\mu_t}{\sigma_\varepsilon}\right)\frac{\partial \varepsilon}{\partial x_j}\right) \quad (9)$$
$$+\left(C_{1\varepsilon}\frac{\varepsilon}{k}(G_k+C_{3\varepsilon}G_b)\right)-\left(C_{2\varepsilon}\rho\frac{\varepsilon^2}{k}+S_k\right) \quad [35]$$

where S_k, S_ε are the source terms, G_k represents the generation of turbulence kinetic energy due to the mean velocity gradients, G_b is the generation of turbulence kinetic energy due to buoyancy, σ_k and σ_ε are Prandtl number of k and ε respectively and μ_t is turbulent viscosity defined by the following equation.

$$\mu_t=\rho C_\mu\frac{k^2}{\varepsilon} \quad [35] \quad (10)$$

C_1, C_2 and C_3 are empirical constants which are given in Table 3.

Table 3 values and constants RNG k-ε model

C_μ	C_1	C_2	C_3	σ_k	σ_ε
0.09	1.44	1.92	1.44	1	1.3

3.2. Boundary and initial conditions

To determine the boundary and initial conditions in Fluent analytical software, first, the physical properties of Table 2 were applied and then the boundary conditions governing the problem were

obtained from Kim et al[31]. The values for the boundary conditions are shown in Table 4. It is noteworthy that in this simulation, the soil temperature is assumed to be constant and an unsteady (transient) solution is presented to solve the problem. Also, the velocity and pressure terms of the momentum equations are discretized by the SIMPLE algorithm.

Table 4 Geometrical parameters

	Quantity	Value
1	Initial soil temperature	283.15(K)
2	Constant flux density in each pipe	300(W/m)
3	Inlet fluid temperature	300(K)
4	Fluid mass flow rate	0.30(kg/s)

3.3. Meshing

A free split tetrahedral mesh was established as illustrated in Figure 2. The mesh on the inlet and outlet edges of the U-shaped pipe and the edges of the borehole are encrypted separately to achieve a mesh skewness of less than 0.8. Also, using this method, in addition to increasing the accuracy of the values obtained for changes in the velocity of working fluid inside the pipe and also changes in heat flux and temperature inside the pipe and on the borehole wall, the number of grids around the pipe can be changed to check the grid independence. In addition, in order to prevent a sudden increase in fluid velocity and temperature, a boundary layer mesh is considered inside the pipe and in the vicinity of the working fluid.

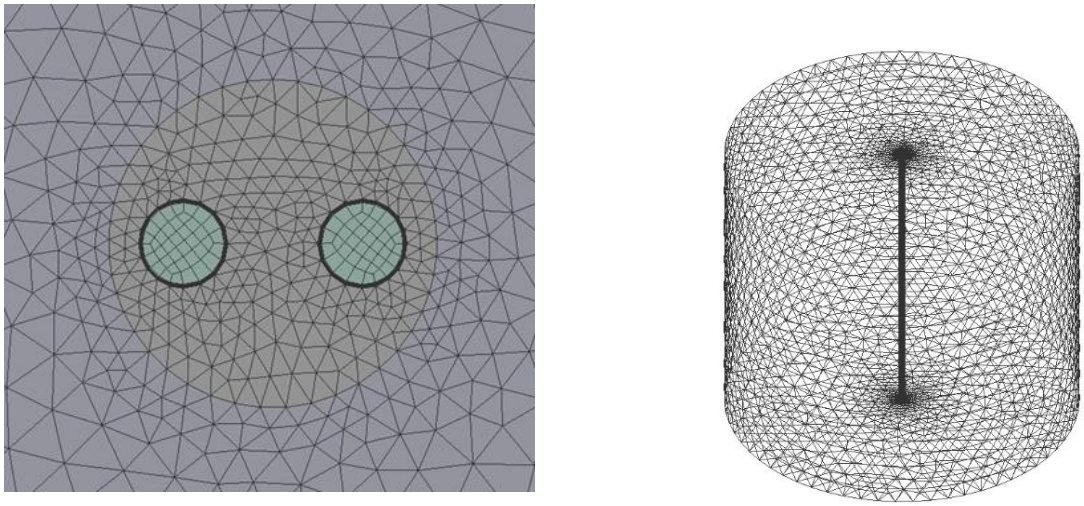

Figure 2 Mesh of the model

4. Validation and grid independence

For numerical simulations, validation and grid independence have been integral steps. Therefore, for validation after applying the initial and boundary conditions and completing the numerical simulation, to ensure the accuracy of the results, temperature changes on the borehole wall were compared with the results of the analytical solution of Kim et al[31]. The results comparison is given in Figure 3.

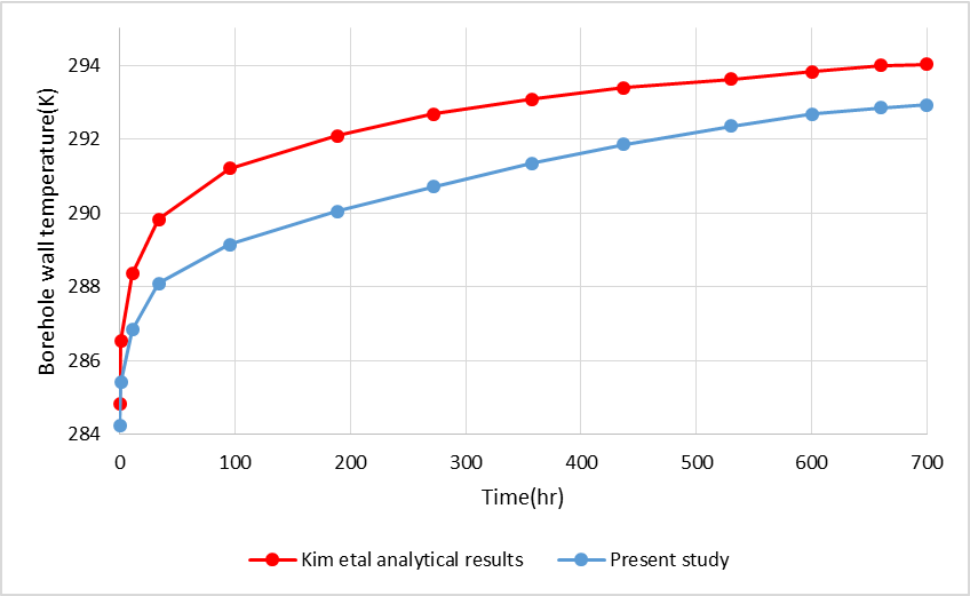

Figure 3 Borehole wall temperature changes comparison between the present study and Kim et. al [31] analytical results.

Comparison of the results obtained from the current CFD solution and the analytical solution performed by Kim et al.[31] showed acceptable agreement and the error between the obtained results and the results of the analytical solution was about 0.6%, which indicates the accuracy of the present numerical solution. In the next step, the grid independence was performed thus, the mesh around the U-tube pipe and borehole wall, which has a significant effect on the results, was gradually made smaller and the temperature at the end of the borehole wall was compared as a specific point. Three different cases were considered to study grid independence. In the first case, the total number of grids was 2 million, in the second case 2.5 million and in the third case 3 million grids were adopted. Temperature values at the end of the borough wall are given in Table 5.

Table 5 Grid independence analysis

	Quantity	Value
1	Case 1	293.68(K)
2	Case 2	292.93(K)
3	Case 3	293.86(K)
4	Analytical results[31]	294.03(K)

What can be seen from Table 5 is that the temperature values for an identical point did not change remarkably with the change in the number of grids. Also, the temperature at the end of the borehole wall values had a suitable agreement with the values obtained in the study by Kim et al[31]. As a result, the grid independence solution has shown the accuracy of numerical simulation.

5. Performance evaluation method

5.1. Heat Load

The heat load value of the BHE system represents the thermal energy released by the water flow through the buried U-shaped pipe and the pipe wall to the surrounding soil or backfill. Thermal performance can be defined by the distribution of thermal load[23], which is directly related to temperature changes at two specific points in the fluid path, for example, the inlet and outlet temperatures can be considered as two points. The heat load is also directly related to the mass flow rate, which is as follows:

$$Q = C_p \times \dot{m} \times (T_{in} - T_{out}) \text{ [26]} \tag{11}$$

Where C_p is specific heat capacity (J/kg.K), Q is assumed as heat load (W), m is the mass flow rate of water (kg/s) and T_{in}, T_{out} is the inlet and outlet temperature of the water. It is noteworthy that since the radius of the U-shaped pipe compare to the surrounding soil is negligible, only the temperature changes of the working fluid inside the pipe along the depth of the pipe (i.e. y direction) were considered[36]. Since the flow regime is turbulent and turbulence intensity affects the forced convection heat transfer, the relation between turbulence intensity and forced convection heat transfer was simulated by the following equations[37].

$$\rho\overline{u_j' u_i'} + \mu_t \left(\frac{\partial u_i}{\partial x_j} + \frac{\partial u_j}{\partial x_i} \right) - \frac{2}{3}\rho k \delta_{ij} - \frac{2}{3}\mu_t \frac{\partial u_k}{\partial x_k}\delta_{ij} \text{ [37]} \tag{12}$$

$$\rho\overline{u_j' u_i'} + \mu_t \left(\frac{\partial u_i}{\partial x_j} + \frac{\partial u_j}{\partial x_i} \right) - \frac{2}{3}\rho k \delta_{ij} - \frac{2}{3}\mu_t \frac{\partial u_k}{\partial x_k}\delta_{ij} \text{ [37]} \tag{13}$$

$$\frac{\partial}{\partial x_i}\left(\rho T u_i\right)=\frac{\partial}{\partial x_i}\left(\left(\Gamma+\Gamma_t\right)\frac{\partial T}{\partial x_i}\right),\left(\Gamma=\frac{\mu}{\mathrm{Pr}}\right),\left(\Gamma_t=\frac{\mu_t}{\mathrm{Pr}_t}\right)\text{[37]} \quad (14)$$

5.2.Backfill properties

The backfill physical and thermal properties such as thermal conductivity and density have a significant effect on the thermal performance of BHE. In order to the insulation of BHE to offset the negative impact of groundwater, a compressed material, which is industrially known as grout, is used to fill the backfill zone. Borehole is considered and designed around the U-shaped pipes. Grout materials can have porosity such as sand, gravel, silt, or clay, but by compacting those materials, the porosity reaches a small negligible amount. As a result, groundwater seepage will be eliminated in this non-porous area. It should be noted, the thermal and physical properties of the grout materials play an important role in the thermal efficiency of BHE[38]. The heat transfer process is launched in impermeable soil by a dry portion of soil and in undrained saturated soil thus, heat transfer is happened by passing of groundwater through this phase. The wet portion of soil will be changed by the fluctuation of weather temperature, and those alterations have consisted of feezing or steaming groundwater [38]. However, in order to simplify the simulation those unforeseeable changes were overlooked. As surrounded soil is involved with thermal resistance, it has an impact on the efficiency of BHE. In this simulation thermal resistance of all effective parts of the system is derived from TRT. As the U-shape pipe is located in the soil domain and backfill has covered it, the thermal resistance of the system is a sum of all thermal resistances together. The total resistance equation is written below.

$$R_{total}=R_f+R_s+R_{grout}\ \text{[38]} \quad (15)$$

$$R_f = \frac{1}{2\pi r_p^i h} \text{ [38]} \quad (16)$$

$$R_p = \frac{1}{2\pi\lambda_p} \ln\left(\frac{r_{eq}^o}{r_{eq}^i}\right) \text{[38]} \quad (17)$$

$$R_{grout} = \frac{1}{2\pi\lambda_{grout}} \ln\left(\frac{r_b}{r_{eq}^o}\right) \text{ [38]} \quad (18)$$

$$h = 0.023\,\mathrm{Re}^{0.8}\,\mathrm{Pr}^{0.35}\,\frac{\lambda_f}{r_i} \text{ [38]} \quad (19)$$

Where R_{total} (m.K/W) is the overall thermal resistance for the entire domain regarding the thermal resistance of the working fluid which is illustrated as R_f (m.K/W), heat resistance of the solid wall of the pipe is shown as R_s (m.K/W) and R_{grout} (m.K/W) is the heat resistance of the filler material of borehole. As well r_p is the U-shaped pipe radius and also r_{eq} is the equivalent pipe radius calculated as $\sqrt{2r_p}$ [32]. Superscripts i and o illustrate the inner and outer parts of pipe/equivalent pipe, respectively, and finally, h is the convective heat transfer coefficient of the operating fluid, which is determined using the Reynolds and Prandtl numbers[38], [39].

6. Results and discussions

6.1. Effect of inlet mass flow rate

In this section, the effect of inlet mass flow rate in order to study the effect of this parameter on thermal energy storage of the ground were investigated. To achieve this aim, three mass flow rates of 0.1(kg/s), 0.3(kg/s) and 0.5(kg/s) were examined. The effective velocity and the Reynolds number increase with increasing inlet mass flow rate. The initial required values for each analysis

stage are given in Table 6. The results of the effect of different mass flow rates on the increase of borehole wall temperature are shown in Figure 4.

Table 6 Specifications of the inlet fluid flow

Quantity(unit)	Inlet mass flow rate(kg/s)	Inlet velocity(m/s)	Reynolds number
1	0.1	0.14	3330
2	0.3	0.44	9990
3	0.5	0.73	16650

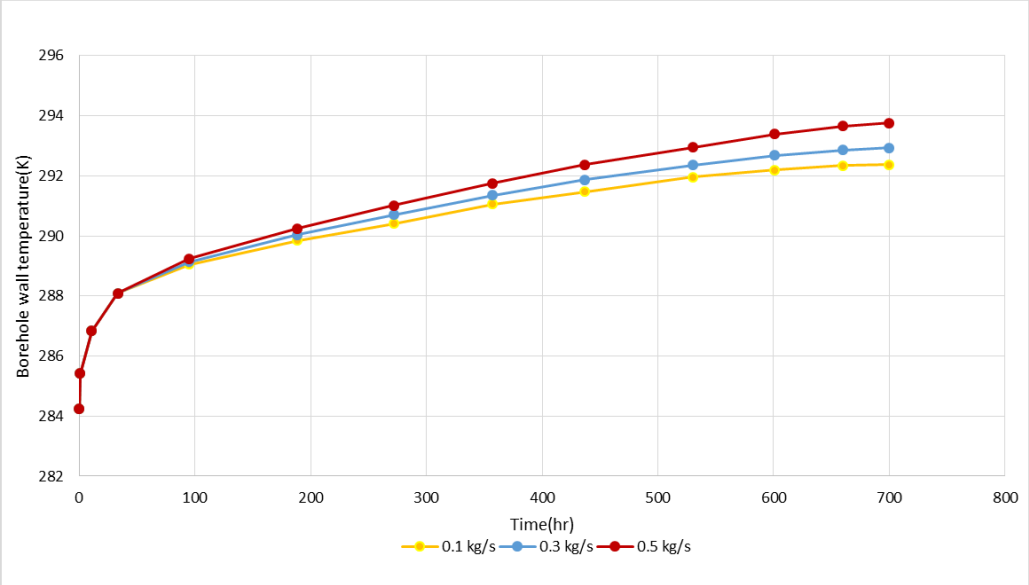

Figure 4 Borehole wall temperature for different mass flow rates

Regarding the details of Table 6, the growth of the mass flow rate was directly related to the inlet velocity. Also, the Reynolds number increased significantly with rising the inlet velocity. According to Equation 24, increasing the Reynolds number leads to an increase in the Nusselt number and the convection heat transfer coefficient. As a result, the phenomenon of forced convection heat transfer inside the U-shaped BHE system has increased, which means more

thermal energy is transferred between the pipe wall and circulating fluid by forced convection. Subsequently, heat is transferred from the pipe wall to the borehole wall through conduction heat transfer. Also, the temperature contours for different mass flow rates at the depth of 2.5 m are shown in Figure 5.

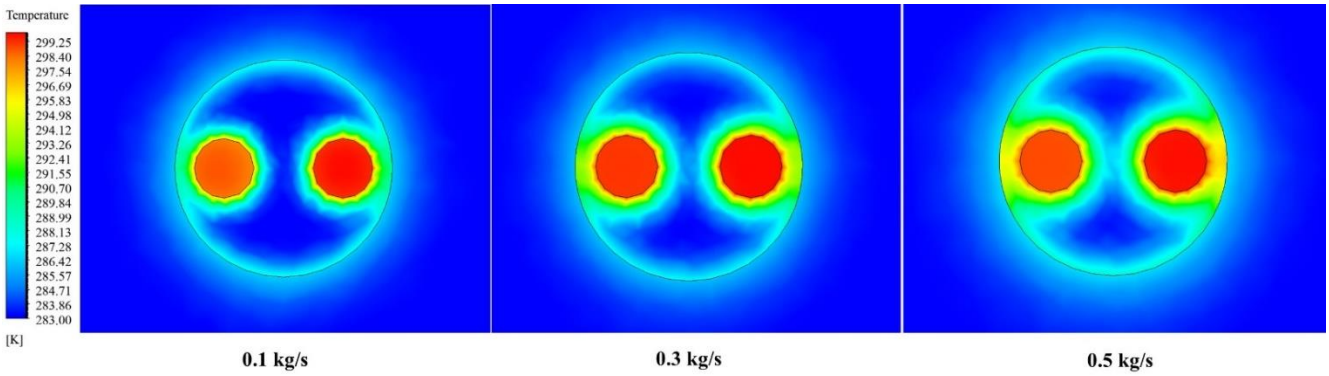

Figure 5 Temperature contours for different mass flow rates

As depicted in Figure 5, it was observed that with the selection of larger mass flow rates, the temperature changes of the borehole wall have increased. This principle indicates that the energy storage performance of the soil is better, and the efficiency of the system is increased. However, it is essential to note that in the early hours, the increase in temperature changes on the borehole wall was not tangible, and over time, where the fluid velocity has increased sufficiently, and the flow is fully developed, these changes have been observed. While studying the effect of inlet mass flow rate on BHE performance, an important issue is the pressure drop in the pipe, which should be investigated. Pressure drop is related to flow velocity and Reynolds number. The pressure drop inside the pipe is calculated from the Darcy-Weissbach equation which is given below.

$$\Delta P_l = \frac{F}{D}\frac{\rho V_{in}^{\ 2}}{2} \text{ [40]} \quad (49)$$

$$F = \frac{0.3164}{\mathrm{Re}^{0.25}} \text{ [40]} \quad (50)$$

$$\Delta P = \Delta P_l \times L \text{ [40]} \quad (51)$$

In the above equations ΔP (kPa) is considered as the pressure drop along the pipe, F is the friction factor and Re is the Reynolds number. Reynolds number values for different inlet mass flow rate values are listed in Table 6. Pressure drop and Reynolds number as a function of mass flow rate are illustrated in Figure 6.

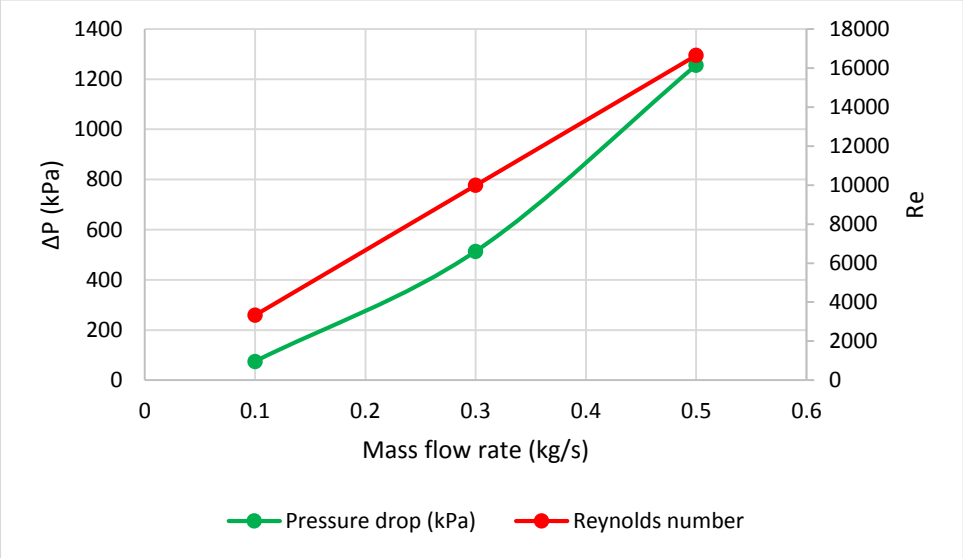

Figure 6 Variations of the pressure drop and Reynolds number as a function of mass flow rate.

Based on the details, when mass flow rate and subsequently inlet velocity increased, Reynolds number and pressure drop along the pipe grew. This unfavorable pressure drop along the pipe can cause a reduction in BHE performance. However, it should be noted that increasing the working

fluid velocity over time can compensate for the negative impact of local friction and pressure drop along the pipe. Also, in order to clarify the pressure and flow field along the whole computational domain, pressure drop and Reynolds number variations along the pipe is calculated. The results are presented in Table 7

Table 7 Variations of the pressure drop and the Reynolds number along the pipe.

		$\dot{m}$=0.1(kg/s)		$\dot{m}$=0.3(kg/s)		$\dot{m}$=0.5(kg/s)	
	L(m)	Re	ΔP(MPa)	Re	ΔP(MPa)	Re	ΔP(MPa)
1	0	3330.09	0	9990.27	0	16650.45	0
2	-0.6	4484.714	8.335	13189.41	56.99	22008.93	139.34
3	-1.1	4514.715	28.065	12834.98	185.36	20564.54	454.12
4	-1.7	4512.602	42.591	12609.09	265.09	20114.29	604.89
5	-2.2	4514.272	56.742	12432.78	342.65	19636.15	775.87
6	-2.8	4516.469	70.973	12293.80	417.89	19195.64	929.85
7	-3.3	4518.731	85.24	12178.19	491.69	18879.47	1072.38
8	-3.9	4521.103	99.534	12079.59	564.24	18654.17	1215.27
9	-4.4	4523.662	113.858	11999.53	635.73	18484.66	1360.01
10	-5	4488.443	128.217	11826.52	706.93	18201.69	1505.76

Regarding the information in Table 7 in general there was an upward trend in both pressure drop and Reynolds number along pipe depth. Increasing Reynolds number values and consequently working fluid velocity growth along pipe depth enhance the efficiency of the system while pressure drop values along pipe depth cause a reduction in system performance, however; the positive effect of Reynolds number increase is more than the pressure drop negative effect. Reynolds number and pressure drop changes at $\dot{m}$=0.5(kg/s) was more remarkable than other situations, the results of pressure drop and Reynolds number variations are illustrated in Figure 7.

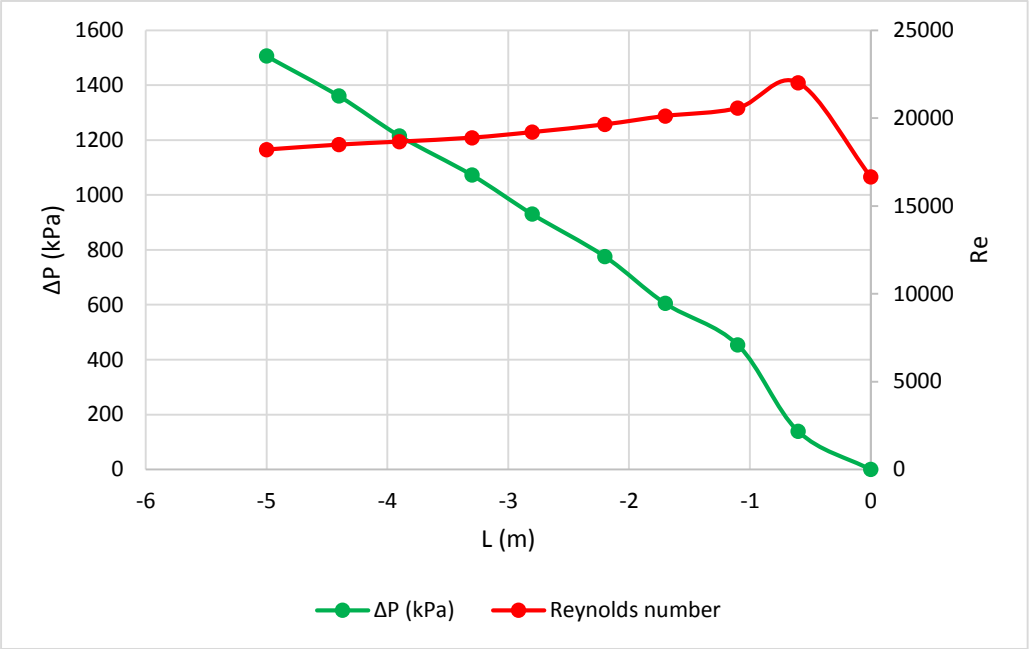

Figure 7 Pressure drop and Reynolds number change along pipe depth.

As for the information in Figure 6 pressure drop and Reynolds number variation along the pipe, are plotted. The Reynolds number increases from the inlet to near the depth of 1 m. From a depth of 1 m to 5 m, the water temperature decreases gradually, resulting in increasing dynamic viscosity of water and a decrease in Reynolds number. The pressure drop has a constant slope as a function of depth. However the pressure drop for each section of the pipe (P_l) is a strong function of fluid velocity and has similar changes.

6.2. Effect of backfill material

The thermal properties of the backfill can play an influential role in the performance of BHE. Therefore, the five commonly used materials for the borehole filling were evaluated and compared, which are given in Table 8.

Table 8 Thermal properties of different backfill materials

	Quantity	Value
1	Grout specific heat	1627(J/kg.K)
2	Grout thermal conductivity	0.8(W/m.K)
3	Sand specific heat	800(J/kg.K)
4	Sand thermal conductivity	1.3(W/m.K)
5	Bentonite specific heat	1627(J/kg.K)
6	Bentonite thermal conductivity	1.3(W/m.K)
7	Clay soil specific heat	2200(J/kg.K)
8	Clay soil thermal conductivity	1.6(W/m.K)
9	Graval specific heat	1627(J/kg.K)
10	Graval thermal conductivity	2.3(W/m.K)

The effect of these materials on borehole wall temperature was examined; the results are shown in Figure 8.

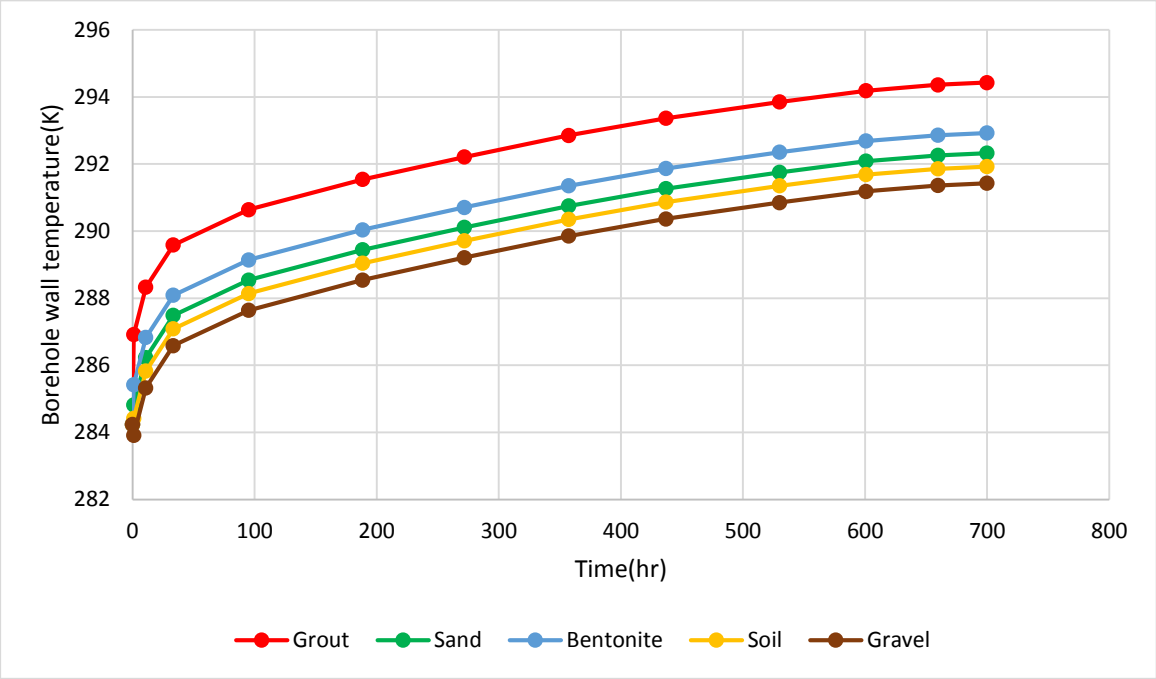

Figure 8 Borehole wall temperature for different backfill materials

It was claimed that the best filling of these five types was grout. The remarkable growth in borehole wall temperature compared to other materials as filling indicates that more heat exchange has taken place between the working fluid and the borehole around the pipe. For better illustration, the temperature contours of different backfill materials at the depth of 2.5 m can be observed in Figure 9.

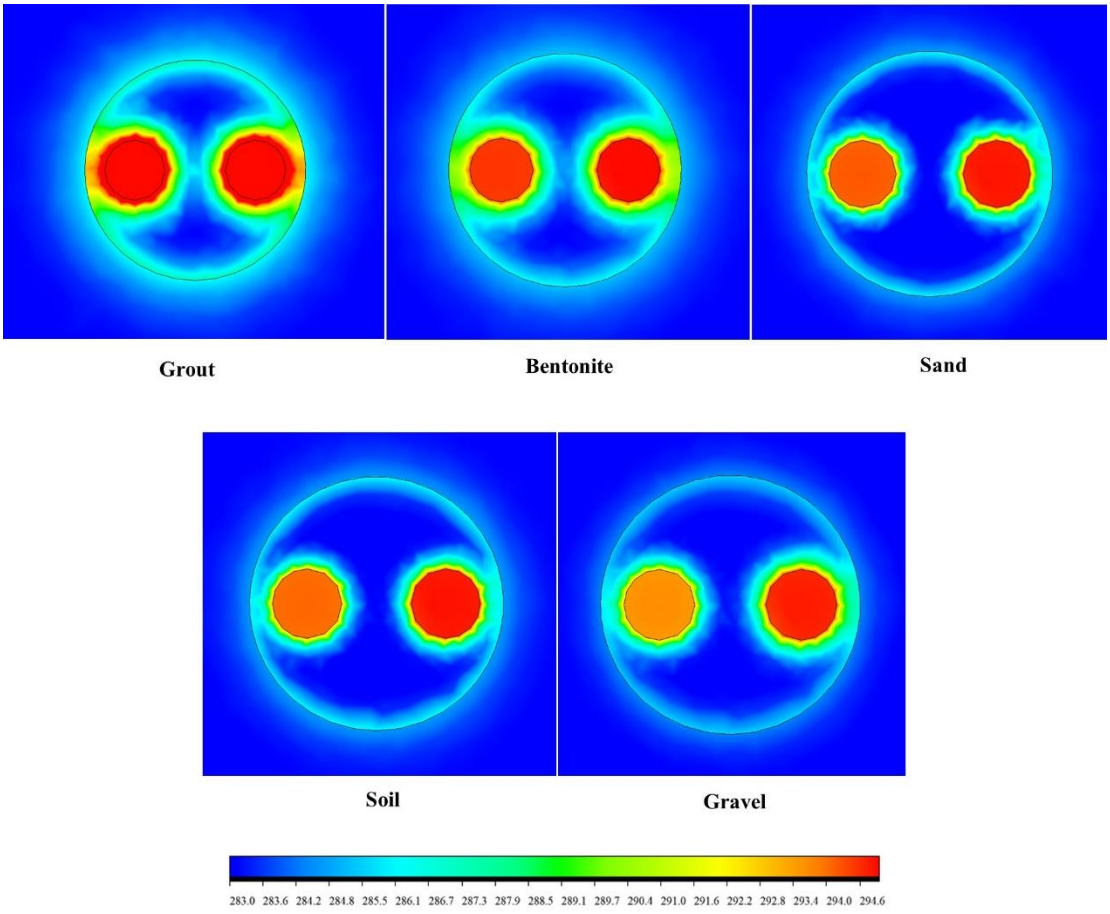

Figure 9 Temperature contours for different backfill materials

As shown in Figure 8, the borehole and the backfill temperature for grout are much higher than other materials due to their lower thermal conductivity which according to the law of heat conduction, for constant heat as thermal conductivity decreases the temperature gradient increases.

Also, the gravel backfill has the lowest temperature gradient around the pipes among the backfill material.

7. Conclusion

Using the CFD method, a U-tube BHE system whose main application was cooling was numerically evaluated. Numerical results showed that the inlet mass flow rate is effective in reducing the temperature of the working fluid. The results showed that the more the inlet mass flow rate increases, the more the temperature of the borehole wall increases, which a mass flow rate of 0.5 (kg/s) indicating more heat exchange between the backfill around the system and the working fluid, as a result, it brings more water temperature reduction. On the other hand, with the passage of time and the increase in the mass flow rate, the pressure drop at the end of the pipe increased, which is an unfavorable phenomenon for the efficiency of the system, however; the positive effect of the increase in the Reynolds number was more than the negative effect of the pressure drop. Also, by examining the type of backfill material with different physical and thermal properties, it was determined that grout is the best material for filling the borehole, and in this case, the temperature of the borehole wall increases the most over time.

References

[1] N. L. Panwar, S. C. Kaushik, and S. Kothari, “Role of renewable energy sources in environmental protection: A review,” *Renewable and Sustainable Energy Reviews*, vol. 15, no. 3, pp. 1513–1524, Apr. 2011, doi: 10.1016/j.rser.2010.11.037.

[2] I. B. Fridleifsson, “Geothermal energy for the benefit of the people,” *Renewable and Sustainable Energy Reviews*, vol. 5, no. 3, pp. 299–312, Sep. 2001, doi: 10.1016/S1364-0321(01)00002-8.

[3] E. Barbier, “Geothermal energy technology and current status: an overview,” *Renewable and Sustainable Energy Reviews*, vol. 6, no. 1–2, pp. 3–65, Jan. 2002, doi: 10.1016/S1364-0321(02)00002-3.

[4] J. W. Lund and A. N. Toth, “Direct utilization of geothermal energy 2020 worldwide review,” *Geothermics*, vol. 90, p. 101915, Feb. 2021, doi: 10.1016/j.geothermics.2020.101915.

[5] M. El Haj Assad, M. H. Ahmadi, M. Sadeghzadeh, A. Yassin, and A. Issakhov, "Renewable hybrid energy systems using geothermal energy: hybrid solar thermal–geothermal power plant," *International Journal of Low-Carbon Technologies*, vol. 16, no. 2, pp. 518–530, May 2021, doi: 10.1093/ijlct/ctaa084.
[6] M. Mahmoud, M. Ramadan, S. Naher, K. Pullen, M. Ali Abdelkareem, and A.-G. Olabi, "A review of geothermal energy-driven hydrogen production systems," *Thermal Science and Engineering Progress*, vol. 22, p. 100854, May 2021, doi: 10.1016/j.tsep.2021.100854.
[7] Y. Wang, F.-Y. Zhao, J. Kuckelkorn, H. Spliethoff, and E. Rank, "School building energy performance and classroom air environment implemented with the heat recovery heat pump and displacement ventilation system," *Applied Energy*, vol. 114, pp. 58–68, Feb. 2014, doi: 10.1016/j.apenergy.2013.09.020.
[8] P. E. Nejad and M. Bernier, "Simulations of a New Double U-tube Borehole Configuration with Solar Heat Injection and Ground Freezing," p. 12.
[9] A. Hepbasli and Y. Kalinci, "A review of heat pump water heating systems," *Renewable and Sustainable Energy Reviews*, vol. 13, no. 6–7, pp. 1211–1229, Aug. 2009, doi: 10.1016/j.rser.2008.08.002.
[10] Q. Zhao, F. Liu, C. Liu, M. Tian, and B. Chen, "Influence of spiral pitch on the thermal behaviors of energy piles with spiral-tube heat exchanger," *Applied Thermal Engineering*, vol. 125, pp. 1280–1290, Oct. 2017, doi: 10.1016/j.applthermaleng.2017.07.099.
[11] Y. Noorollahi, M. Pourarshad, S. Jalilinasrabady, and H. Yousefi, "Numerical simulation of power production from abandoned oil wells in Ahwaz oil field in southern Iran," *Geothermics*, vol. 55, pp. 16–23, May 2015, doi: 10.1016/j.geothermics.2015.01.008.
[12] A. Eswiasi and P. Mukhopadhyaya, "Performance of Conventional and Innovative Single U-Tube Pipe Configuration in Vertical Ground Heat Exchanger (VGHE)," *Sustainability*, vol. 13, no. 11, p. 6384, Jun. 2021, doi: 10.3390/su13116384.
[13] M. Mahmoud *et al.*, "A review of grout materials in geothermal energy applications," *International Journal of Thermofluids*, vol. 10, p. 100070, May 2021, doi: 10.1016/j.ijft.2021.100070.
[14] L. Alberti, A. Angelotti, M. Antelmi, and I. La Licata, "A Numerical Study on the Impact of Grouting Material on Borehole Heat Exchangers Performance in Aquifers," *Energies*, vol. 10, no. 5, p. 703, May 2017, doi: 10.3390/en10050703.
[15] H. Wang, C. Qi, H. Du, and J. Gu, "Improved method and case study of thermal response test for borehole heat exchangers of ground source heat pump system," *Renewable Energy*, vol. 35, no. 3, pp. 727–733, Mar. 2010, doi: 10.1016/j.renene.2009.08.013.
[16] A. Galgaro, G. Dalla Santa, and A. Zarrella, "First Italian TRT database and significance of the geological setting evaluation in borehole heat exchanger sizing," *Geothermics*, vol. 94, p. 102098, Jul. 2021, doi: 10.1016/j.geothermics.2021.102098.
[17] T. V. Bandos *et al.*, "Finite line-source model for borehole heat exchangers: effect of vertical temperature variations," *Geothermics*, vol. 38, no. 2, pp. 263–270, Jun. 2009, doi: 10.1016/j.geothermics.2009.01.003.
[18] A.-M. Gustafsson, L. Westerlund, and G. Hellström, "CFD-modelling of natural convection in a groundwater-filled borehole heat exchanger," *Applied Thermal Engineering*, vol. 30, no. 6–7, pp. 683–691, May 2010, doi: 10.1016/j.applthermaleng.2009.11.016.
[19] T. Renaud, P. Verdin, and G. Falcone, "Numerical simulation of a Deep Borehole Heat Exchanger in the Krafla geothermal system," *International Journal of Heat and Mass Transfer*, vol. 143, p. 118496, Nov. 2019, doi: 10.1016/j.ijheatmasstransfer.2019.118496.

[20] R. Saeidi, Y. Noorollahi, and V. Esfahanian, "Numerical simulation of a novel spiral type ground heat exchanger for enhancing heat transfer performance of geothermal heat pump," *Energy Conversion and Management*, vol. 168, pp. 296–307, Jul. 2018, doi: 10.1016/j.enconman.2018.05.015.
[21] D. Gordon, T. Bolisetti, D. S.-K. Ting, and S. Reitsma, "Experimental and analytical investigation on pipe sizes for a coaxial borehole heat exchanger," *Renewable Energy*, vol. 115, pp. 946–953, Jan. 2018, doi: 10.1016/j.renene.2017.08.088.
[22] S. E. Dehkordi, R. A. Schincariol, and S. Reitsma, "Thermal performance of a tight borehole heat exchanger," *Renewable Energy*, vol. 83, pp. 698–704, Nov. 2015, doi: 10.1016/j.renene.2015.04.051.
[23] G. Li, J. Yang, X. Zhu, and Z. Shen, "Numerical study on the heat transfer performance of coaxial shallow borehole heat exchanger," *Energy and Built Environment*, vol. 2, no. 4, pp. 445–455, Oct. 2021, doi: 10.1016/j.enbenv.2020.10.002.
[24] D. Pahud and B. Matthey, "Comparison of the thermal performance of double U-pipe borehole heat exchangers measured in situ," *Energy and Buildings*, vol. 33, no. 5, pp. 503–507, May 2001, doi: 10.1016/S0378-7788(00)00106-7.
[25] B. Bouhacina, R. Saim, H. Benzenine, and H. F. Oztop, "Analysis of thermal and dynamic comportment of a geothermal vertical U-tube heat exchanger," *Energy and Buildings*, vol. 58, pp. 37–43, Mar. 2013, doi: 10.1016/j.enbuild.2012.11.037.
[26] L. Zhu, S. Chen, Y. Yang, and Y. Sun, "Transient heat transfer performance of a vertical double U-tube borehole heat exchanger under different operation conditions," *Renewable Energy*, vol. 131, pp. 494–505, Feb. 2019, doi: 10.1016/j.renene.2018.07.073.
[27] J. Liu *et al.*, "Influencing factors analysis and operation optimization for the long-term performance of medium-deep borehole heat exchanger coupled ground source heat pump system," *Energy and Buildings*, vol. 226, p. 110385, Nov. 2020, doi: 10.1016/j.enbuild.2020.110385.
[28] G. Diglio, C. Roselli, M. Sasso, and U. Jawali Channabasappa, "Borehole heat exchanger with nanofluids as heat carrier," *Geothermics*, vol. 72, pp. 112–123, Mar. 2018, doi: 10.1016/j.geothermics.2017.11.005.
[29] J. Liu, F. Wang, W. Cai, Z. Wang, and C. Li, "Numerical investigation on the effects of geological parameters and layered subsurface on the thermal performance of medium-deep borehole heat exchanger," *Renewable Energy*, vol. 149, pp. 384–399, Apr. 2020, doi: 10.1016/j.renene.2019.11.158.
[30] H. Wang, C. Qi, H. Du, and J. Gu, "Thermal performance of borehole heat exchanger under groundwater flow: A case study from Baoding," *Energy and Buildings*, vol. 41, no. 12, pp. 1368–1373, Dec. 2009, doi: 10.1016/j.enbuild.2009.08.001.
[31] E.-J. Kim, J.-J. Roux, G. Rusaouen, and F. Kuznik, "Numerical modelling of geothermal vertical heat exchangers for the short time analysis using the state model size reduction technique," *Applied Thermal Engineering*, vol. 30, no. 6–7, pp. 706–714, May 2010, doi: 10.1016/j.applthermaleng.2009.11.019.
[32] A. Bejan and A. D. Kraus, *Heat transfer handbook*. New York: J. Wiley, 2003.
[33] S.V. Patankar, *Numerical Heat Transfer and Fluid Flow*.
[34] R. H. Nichols, "Turbulence Models and Their Application to Complex Flows," p. 214, Apr. 2010.
[35] G. C. Papageorgakis, D. N. Assanis, "COMPARISON OF LINEAR AND NONLINEAR RNG-BASED k-epsilon MODELS FOR INCOMPRESSIBLE TURBULENT FLOWS,"

Numerical Heat Transfer, Part B: Fundamentals, vol. 35, no. 1, pp. 1–22, Feb. 1999, doi: 10.1080/104077999275983.

[36] R. Fan, Y. Jiang, Y. Yao, D. Shiming, and Z. Ma, "A study on the performance of a geothermal heat exchanger under coupled heat conduction and groundwater advection," *Energy*, vol. 32, no. 11, pp. 2199–2209, Nov. 2007, doi: 10.1016/j.energy.2007.05.001.

[37] M. Sheikholeslami, M. Jafaryar, D. D. Ganji, and Z. Li, "Exergy loss analysis for nanofluid forced convection heat transfer in a pipe with modified turbulators," *Journal of Molecular Liquids*, vol. 262, pp. 104–110, Jul. 2018, doi: 10.1016/j.molliq.2018.04.077.

[38] J. C. Choi, J. Park, and S. R. Lee, "Numerical evaluation of the effects of groundwater flow on borehole heat exchanger arrays," *Renewable Energy*, vol. 52, pp. 230–240, Apr. 2013, doi: 10.1016/j.renene.2012.10.028.

[39] J. Dirker and J. P. Meyer, "Convective Heat Transfer Coefficients in Concentric Annuli," *Heat Transfer Engineering*, vol. 26, no. 2, pp. 38–44, Mar. 2005, doi: 10.1080/01457630590897097.

[40] Y. Huang, Y. Zhang, Y. Xie, Y. Zhang, X. Gao, and J. Ma, "Long-term thermal performance analysis of deep coaxial borehole heat exchanger based on field test," *Journal of Cleaner Production*, vol. 278, p. 123396, Jan. 2021, doi: 10.1016/j.jclepro.2020.123396.